Carbon Trends 9 (2022) 100216

Contents lists available at ScienceDirect

Carbon Trends

journal homepage: www.elsevier.com/locate/cartre

High entropy alloy nanoparticle - graphene (HEA:G) composite for non-enzymatic glucose oxidation : optimization for enhanced catalytic performance

R. Ashwini[a], M.K. Punith Kumar[b], M.Y. Rekha[c], M.S. Santosh[d], Chandan Srivastava[b,*]

[a] Centre for Incubation, Innovation, Research and Consultancy (CIIRC), Jyothy Institute of Technology (affiliated to VTU), Tataguni, Off Kanakapura Road, Bengaluru 560082, Karnataka, India
[b] Department of Materials Engineering, Indian Institute of Science, C.V. Raman Road, Bengaluru 560012, Karnataka, India
[c] Department of Metallurgical and Materials Engineering, The University of Alabama, Tuscaloosa, AL, United States
[d] Coal and Mineral Processing Division, CSIR, Central Institute of Mining and Fuel Research (CIMFR), Digwadi campus, PO: FRI, Dhanbad 828108, Jharkhand, India

ARTICLE INFO

Article history:
Received 3 August 2022
Revised 23 August 2022
Accepted 15 September 2022

Keywords:
Electrochemistry
High entropy alloy – graphene (HEA:G) composite
Electro-catalysis
Non-enzymatic electrochemical sensor
Ball milling

ABSTRACT

High entropy alloy (HEA) metal nanoparticles engineered graphene composites (HEA:G) were produced via green approach involving mechanical milling and sonication assisted exfoliation. Mixture of metal powders and graphite (metal-to-graphite weight ratio: 20%, 50%, 70%, 90%) were ball milled and exfoliated. As produced 20:80, 50:50, 70:30, 90:10 - HEA:G composites electrochemical activity was explored using the redox probe potassium ferricyanide [$K_3Fe(CN)_6$] and for the non-enzymatic detection of glucose. From cyclic voltammetry(CV) response, the significant electron transfer kinetics for $K_3Fe(CN)_6$ was found for 20:80, 50:50, 70:30 composites, whereas reduced activity was observed with 90:10. Also, 20:80, 50:50, 70:30 composites exhibited notable oxidation of glucose in 0.1 M PBS compared to 90:10. The anodic current indicating oxidation of glucose was found to be increasing linearly with HEA:G composite - 20:80<50:50<70:30. However, DPV measurements indicate better working potential from 0.45 V to 0.4 V followed by saturation in the oxidation currents for 50:50 and 70:30 composites. The sensitivity obtained for HEA:G composites 20:80, 50:50, 70:30 were 12.09 $\mu AmM^{-1}cm^{-2}$, 22.99 $\mu AmM^{-1}cm^{-2}$, 18.2 $\mu AmM^{-1}cm^{-2}$ respectively. Hence, 50:50 and 70:30 are the efficient composites exhibiting excellent catalytic activity indicating the prominence of HEA:Graphene composites and their synergism.

1. Introduction

Graphene, a 2D honeycomb structure has emerged as an effective substrate for functional materials, as the host graphene exhibits a large surface area, chemical inertness, and high electrical conductivity [1]. The integration of a variety of nanoparticles with graphene nano-sheets has also been explored in a variety of applications such as energy storage, photocatalysis, electrocatalysis, drug delivery, energy harvesting, etc., [2–6]. Metals possess higher catalytic activity at the nanoscale, however, compared to un-supported metal nanoparticles, graphene-supported metal nanoparticles acquire enhanced stability and exhibit improved catalytic properties [5–8]. Therefore, the decoration of metal or metal oxide nanoparticles over a graphene nanosheet yields nanocomposites of synergistically augmented electron transfer properties with large active surface area, which makes graphene-nanoparticle composites ideal materials for electrochemical applications [9,10].

Noble metal nanoparticles integrated graphene sheets have garnered significant attention in electrocatalysis [11] and green energy applications because of their unique physical and chemical properties [12]. Yet, commercial applications of noble metal nanoparticles are limited due to their availability and their high costs. Therefore, the use of non-precious, low-cost, and easily available 3-d block transition metal nanoparticles is more viable for catalytic applications [13].

Alternatively, individual metal or alloy nanoparticles are being doped with graphene for better electrocatalytic properties [14, 15]. In recent times, alloy nanoparticles with five principal elements of nearly equimolar concentration also known as High Entropy Alloy (HEA) nanoparticles have gained substantial attention

* Corresponding author.
E-mail address: csrivastava@iisc.ac.in (C. Srivastava).

https://doi.org/10.1016/j.cartre.2022.100216

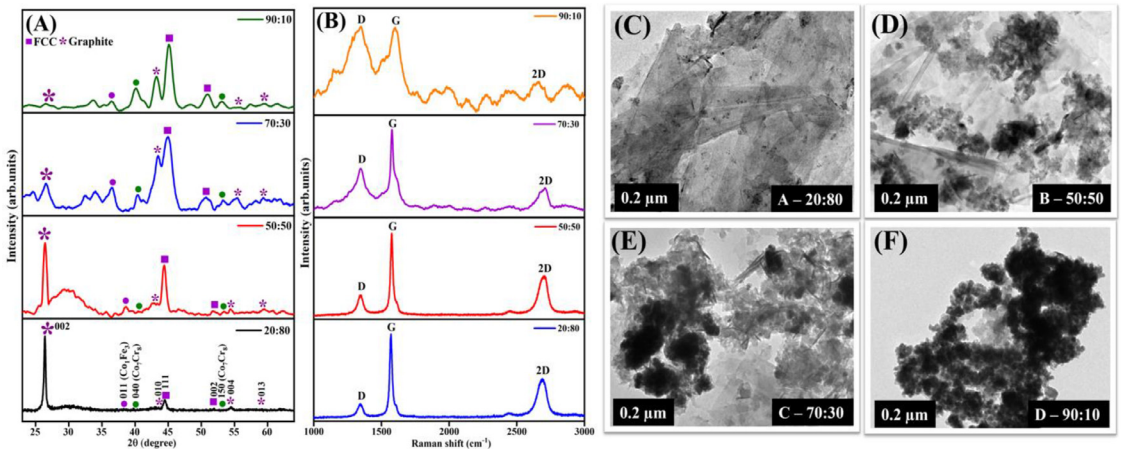

Fig. 1. (A) - XRD patterns obtained for HEA:G composites – 20:80, 50:50, 70:30 and 90:10 indicating the formation of single-phase (FCC) HEA nanoparticles, (B) Raman spectra obtained for HEA:G composites – 20:80, 50:50, 70:30 and 90:10 indicating an increase in defect density with increase in a weight ratio of HEA nanoparticle. (C - D) High magnification TEM images representing HEA nanoparticles distribution on graphene sheets for different HEA:G composites.

Table 1
Representing the calculated parameters from XRD and Raman measurements.

HEA: G composite	FWHM (Degree)	Average crystalline size (nm)	Defect density (I_D/I_G ratio)	I_G/I_{2D} ratio	L_a (nm)AverageCrystalline size
20:80	0.50	16 nm	0.2	2	96.12
50:50	0.62	14 nm	0.3	1.98	64.08
70:30	1.50	8 nm	0.71	1.76	27.07
90:10	0.85	10 nm	1.51	1.23	12.73

due to their remarkable mechanical and electrochemical properties [16,17]. HEA nanoparticles have exhibited better intrinsic catalytic activity compared to conventional metal nanoparticles and are extensively explored in energy storage applications. [18,19]. Also, assimilation of HEA nanoparticles over carbon allotropes or graphene synergistically exhibits enhanced capacitance in energy storage devices, higher efficiency in oxygen evolution reaction (OER), and superior corrosion resistance properties compared to solitary/standalone HEA nanoparticles [20–23].

In general, a two-step process is employed to load HEA nanoparticles on the graphene nanosheets. The graphene or reduced graphene oxide (rGO) produced from chemically reduced graphene oxide (GO) is used as a substrate to load HEA nanoparticles by linking organic reagents resulting in HEA/graphene composites [18,24,25]. This process is more favorable to load a higher percentage of nanoparticles on the graphene substrate [26]. However, excessive reagents used in the synthesis of graphene or rGO and the organic molecules utilized to link nanoparticles on graphene surface possibly mask the available catalytic active sites on HEA/graphene composites leading to the diminished catalytic property [27]. Further, as the charge transfer in nanoparticle-graphene composites occurs across the graphene and nanoparticles interface, the presence of any impurities blocks these active sites that are responsible for electron transfer kinetics resulting in the sluggish electrocatalytic activity of the material [28]. Therefore, many efforts have been made to produce nanoparticles blended with graphene composites using a greener approach [29–32].

The present work also employs a two-step green approach i.e., mechanical milling of non-noble principal metal powders [Ni, Fe, Cr, Co, Cu] with graphite followed by an ultrasonic exfoliation process resulting in non-noble HEA nanoparticles loaded graphene nanocomposite (HEA/Graphene). As-synthesized composite's electrochemical kinetic behavior was evaluated using the redox probe potassium ferricyanide [$K_3Fe(CN)_6$]. Except for our recent report on the non-enzymatic urea detection on HEA-Graphene nanocomposite [33], the electrochemical sensing ability of HEA decorated graphene composites is an unexplored area. Hence, the efficiency of the produced HEA:G nanocomposites was evaluated by subjecting the synthesized materials to simple, non-enzymatic electrochemical glucose sensing applications as a proof of concept.

2. Experimental

2.1. Materials

Graphite powder of 99.99% purity and non-noble transition metal powders [nickel (Ni), chromium (Cr), copper (Cu), cobalt (Co) and iron (Fe)] were purchased from Alfa Aesar (India) chemicals. Glucose and phosphate buffer tablets (pH 7.4), used for electrochemical studies were procured from Sigma-Aldrich (Merck, India). The working solutions for electrochemical measurements were prepared by diluting the glucose stock solution with phosphate buffer solution prepared in Millipore water. All the chemicals used in this study were analytical-grade chemicals and were used without further purification.

2.2. Synthesis of HEA:G nanocomposites

Equimolar concentrations of mixed Ni, Cr, Cu, Co and Fe metal powders were used to obtain high entropy alloy (HEA) nanoparticle composition. The different weight percentages of mixed metal powders were blended with the corresponding balancing weight percent of high purity graphite [metal powder-to-graphite weight% ratio - 20:80, 50:50, 70:30 and 90:10] to produce high entropy alloy nanoparticle - Graphene (HEA:G) nanocomposites. Metal powders and graphite blends were subjected to mechanical milling for 100 h in hard chromium steel vials with a ball-to-powder ratio of 20:1. The Milling process was carried out in the presence of toluene as the supporting media. Finally, the milled HEA:Graphite mixtures were separately dispersed in ethanol containing 20 mg of sodium lauryl sulfate (SLS) surfactant followed by ultrasonication for 2 h to facilitate the exfoliation of HEA intercalated graphene

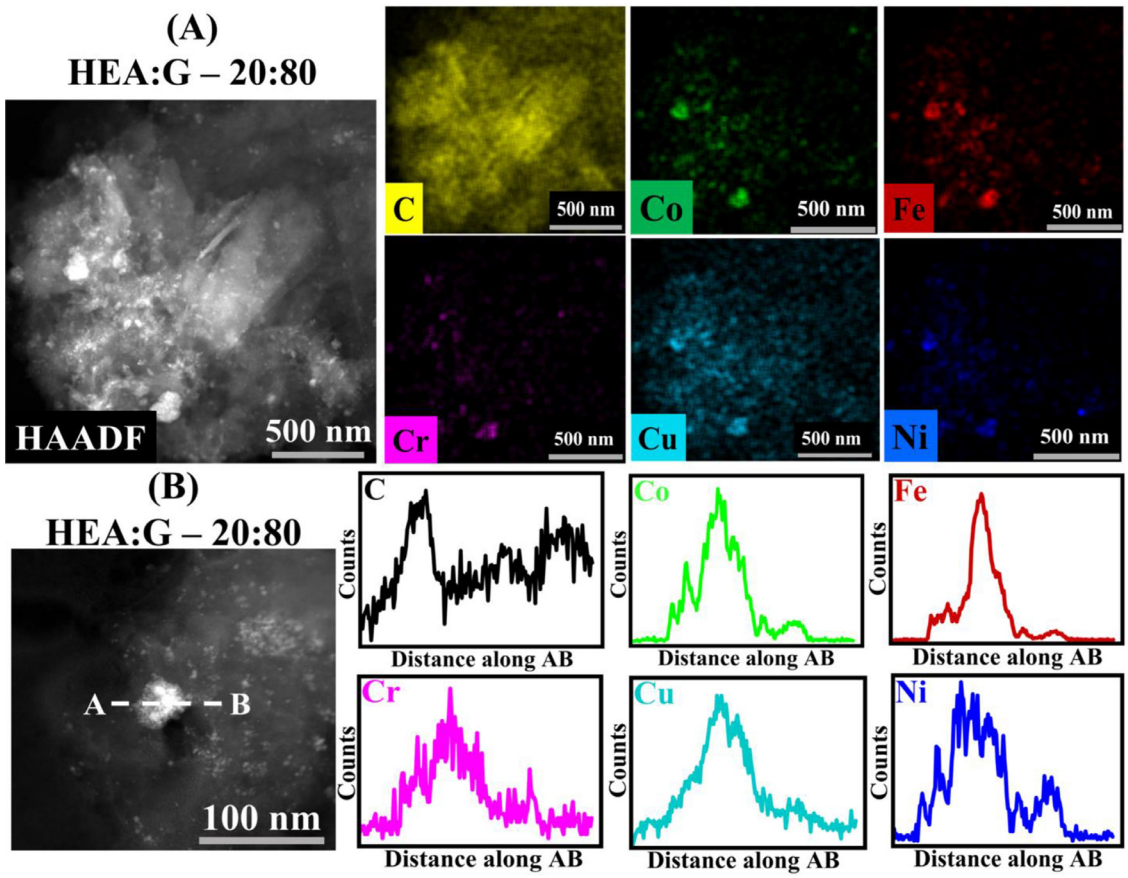

Fig. 2. Representative of HAADF – TEM (A) - compositional mapping and (B) - line profiles obtained for HEA-G composite – 20:80 confirming the presence of constituents (Co, Fe, Cr, Cu, Ni) of HEA nanoparticle on graphene (C).

layers. The HEA:G composites were thoroughly washed with water through centrifugation to eliminate SLS from the resultant composite. The as-produced HEA:G composites are henceforth referred to as 20:80, 50:50, 70:30 and 90:10.

2.3. Material characterization

The phases in as-prepared HEA:G nanocomposites were examined using X-ray diffractograms (XRD) recorded using a X-Pert Pro-X-ray diffractometer and a Cu k radiation source. Defect density in the graphene sheets was studied by Raman spectra obtained from the LabRam HR instrument with a laser operating at 532 nm. Images and composition of the HEA:G composites were obtained using the Titan transmission electron microscope (TEM) instrument with scanning transmission electron microscopy-energy dispersive spectroscopy (STEM-EDS) detector.

2.4. Electrochemical characterization

Electrochemical characteristics of HEA:G nanocomposites for the redox probe $K_3Fe(CN)_6$ and towards non-enzymatic glucose detection were measured using Bio-Logic SP150 electrochemical workstation. Cyclic voltammetry (CV) and differential pulse voltammetry (DPV) techniques were utilized to analyze the electrochemical characteristics of the as-prepared nanocomposites. All the experiments were carried out on a screen-printed electrode (SPE) (Metrohm) which was built with carbon-based working (3 mm) and counter electrodes along with silver as the reference electrode system. The HEA:G composite dispersion of 1 mg/ml were prepared and 10 µl of this dispersion was precisely drop casted on the SPE working electrode area to analyze the electrochemical properties using the redox probe $K_3Fe(CN)_6$ and towards non-enzymatic glucose detection. CV measurements were carried out between the potential range of −0.4 to +0.4 for redox probe $K_3Fe(CN)_6$ in 0.1 M KCl as supporting electrolyte. Whereas for glucose oxidation the potential range was maintained between −0.8 to +0.8 at different scan rates (10 mV/s to 50 mV/s) and different concentrations of glucose (10 mM to 50 mM) in 0.1 M PBS. All the experiments were repeated 3 times to ensure the reproducibility of the results from the HEA:G nanocomposites modified SPE electrode.

3. Results and discussion

3.1. Structural characterization

3.1.1. X-ray diffraction and Raman studies

XRD patterns for HEA:G nanocomposites - 20:80, 50:50, 70:30 and 90:10 are shown in Fig. 1A. The diffraction peak at $2\theta = 26.25^{o}$ corresponds to the (002) plane of a few layered graphene [32]. Higher intensity of the graphitic peak at $2\theta = 26.25^{o}$ (002) is observed for the 20:80 and 50:50 - HEA:G composite whereas for the 70:30 and 90:10 - HEA:G composite, the decrease in the peak intensity indicates a decrease in the volume fraction of graphene content due to increased HEA nanoparticle incorporation. Presence of face-centered cubic (FCC) phase diffraction peaks in the XRD pattern indicates the formation of solid solution between the different component metal atoms (Ni, Cu, Co, Cr, Fe). The diffraction peak at $2\theta = 42.53^{o}$ corresponds to (010) hexagonal graphitic in-plane structure. Broadness of the FCC (111) peak increased with increase in the weight percentage of

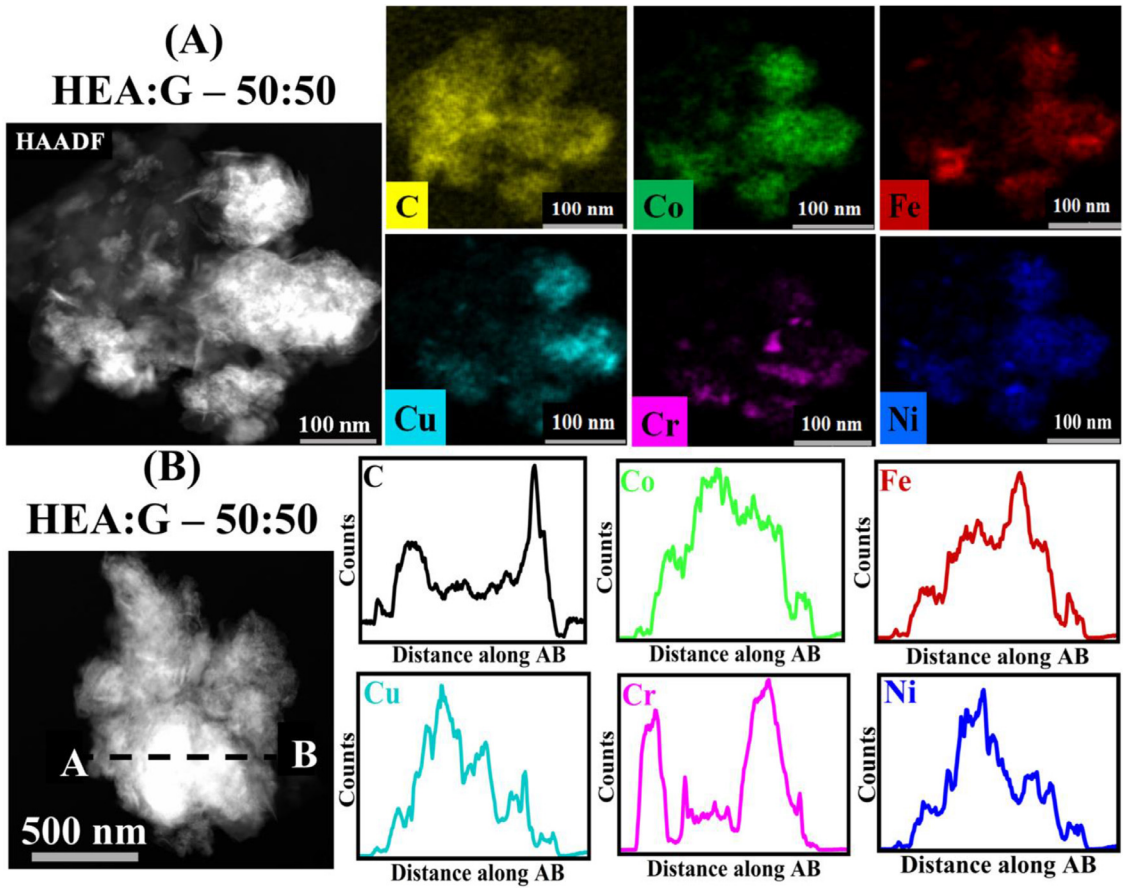

Fig. 3. Representative of HAADF – TEM (A) - compositional mapping and (B) - line profiles obtained for HEA-G composite – 50:50 confirming the presence of constituents (Co, Fe, Cr, Cu, Ni) of HEA nanoparticle on graphene (C).

metal powder indicating a decrease in particle size with increased particle loading on graphene. The Debey – Scherrer [34] formula provided in Eq. (1) was used to calculate the average crystalline size of the HEA nanoparticles.

$$D = k\lambda/\beta cos\theta \quad (1)$$

D = crystalline size (nm), K = constant (0.9), λ = wavelength of X-ray used (1.54×10^{-10}), θ = angle of diffraction and the β = full-width half maxima (FWHM) of the FCC (111) peak. The calculated crystalline size for HEA:G composites are given in Table 1. The bi-metallic phases [Co_1Fe_3, Co_7Cr_8] matches with the standard peaks corresponding to JCPDS card no. 98–010–8312 and 98–007–1327 respectively.

The Raman spectrum in Fig. 1B shows the characteristic peaks of exfoliated few-layered graphene in HEA:G composites. The three characteristic D, G and 2D peaks are at 1346 cm^{-1}, 1575 cm^{-1}, 2700 cm^{-1} respectively. The G - graphitic peak and the 2D peak correspond to the first and second order sp^2 domain phonon vibrations respectively, whereas the D peak is associated with defects on graphene sheets. The intensity of the D peak is increasing linearly with HEA:G composites from 20:80 to 90:10. The defect density (I_D/I_G ratio) for the HEA:G composites (Table 1) is in the order 20:80<50:50<70:30<90:10 indicating a significant increase in the anchoring of HEA nanoparticles on graphene sheets. The characteristic nature of D and G peaks in the composites 70:30 and 90:10 is upshifted compared to that in 50:50 and 20:80. The upshifting of peaks is due to an increased percentage of HEA nanoparticle loading which leads to improved interaction and intercalation of nanoparticles between graphene layers. This contributes towards further exfoliation of graphene layers which is supported by the reduction of I_G/I_{2D} ratio (Table 1) in HEA:G composites. The intensity ratios of G and 2D peak provide information on the number of layers in the exfoliated graphene and reduction in the ratio indicate that graphene is few-layered [35–37]. The mechanical milling process not only contributes to the creation of defects but also towards the reduction of the average crystalline size of the sp^2 domains [La (nm)]. The average crystalline size was calculated and provided in Table 1 using the equation given by Lucchese et al. [27,38]:

$$L_a(nm) = \left(2.4 \times 10^{-10}\right)\lambda^4 (I_D/I_G)^{-1} \quad (2)$$

where L_a is the average crystalline size, λ (nm) wavelength of laser light used – 532 nm. A significant decline in the average crystalline size of the sp^2 domains was observed in HEA:G nanocomposites in the order 20:80>50:50>70:30>90:10. The decrease in the average crystalline size indicates that the mechanical milling process substantially increased the incorporation of HEA particles into the defects in the graphitic layers.

3.1.2. Transmission electron microscopy (TEM)

Representative TEM micrograph of the HEA:G composites – 20:80, 50:50, 70:30, 90:10 are shown in Figs. 1C-1F respectively. The distribution of HEA nanoparticles on the exfoliated few-layered graphene sheets is evident concerning the increase in the particle loading (20 wt%, 50 wt%, 70 wt%, 90 wt%) corresponding to a decrease in the graphene content (80 wt%, 50 wt%, 30 wt%, 10 wt%). The higher percentage of HEA nanoparticle incorporation dominate graphene sheets in composites 70:30 (Fig. 1E) and 90:10 (Fig. 1F) when compared to 20:80 and 50:50. Figs 2A-5A shows STEM-high angle annular dark field (HADDF) images and elemental composi-

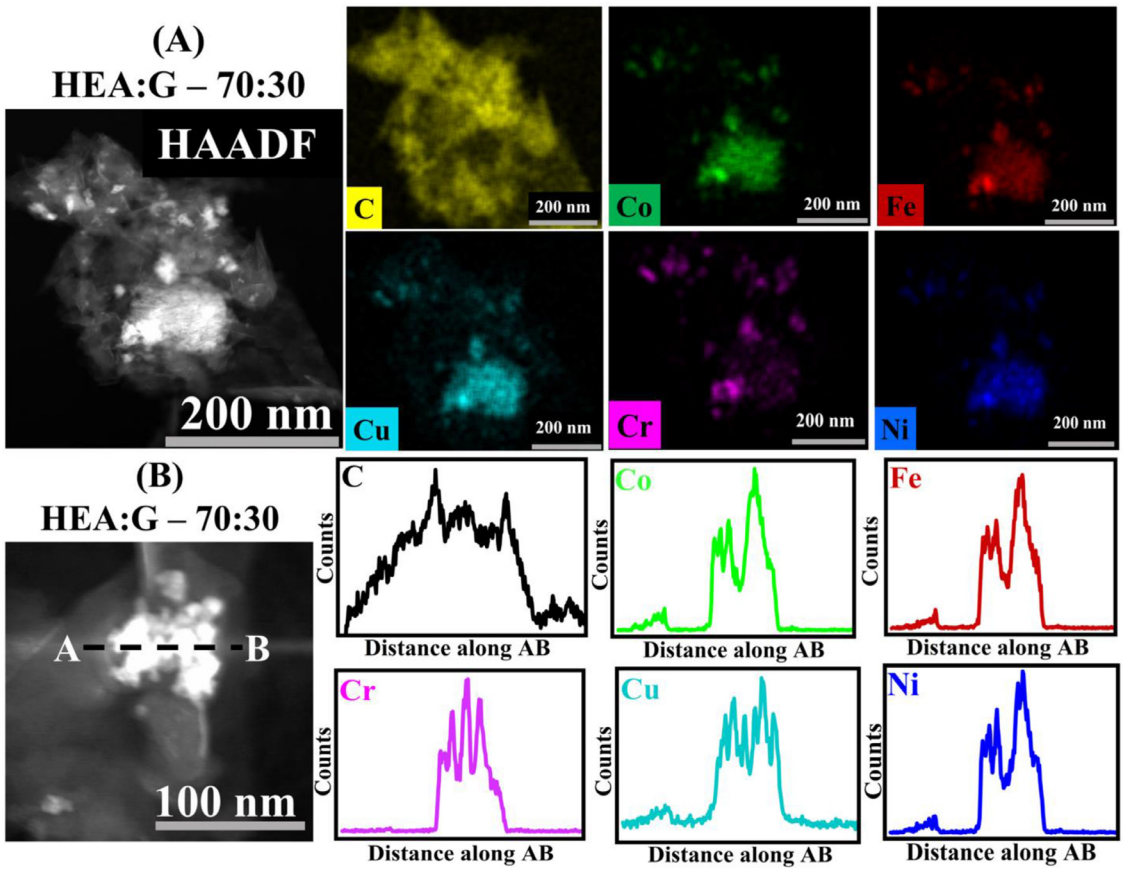

Fig. 4. Representative of HAADF – TEM (A) - compositional mapping and (B) - line profiles obtained for HEA-G composite – 70:30 confirming the presence of constituents (Co, Fe, Cr, Cu, Ni) of HEA nanoparticle on graphene (C).

tional maps obtained from composites. Figs. 2B-5B show the line mapping over the regions of interest for the composites 20:80, 50:50, 70:30 and 90:10 respectively. Both the compositional maps and the compositional line scans clearly show the presence of all the component elements in the nanoparticles.

3.2. Electrochemical characterization

The electro-chemical behavior of the as-produced HEA:G composites were investigated for the redox probe potassium ferricyanide [$K_3Fe(CN)_6$] and catalytic activity towards the electro-oxidation of glucose using cyclic voltammetry (CV) and differential pulse voltammetry (DPV) techniques. The screen printed electrodes (SPE) modified with HEA:G composite was used to perform CV in 2 mM $K_3Fe(CN)_6$ in 0.1 M KCl as the supporting electrolyte at different scan rates from 10 mV/s to 50 mV/s. Figs.6A - 6D show the cyclic voltammogram response obtained for the composites 20:80, 50:50, 70:30 and 90:10 respectively for the redox probe $K_3Fe(CN)_6$. As the scan rate increased, the oxidation and reduction potential increased linearly for all the composites indicating that the electrochemical process is quasi-reversible. The peak-to-peak separation potentials [ΔE_p] indicates the rate of electron transfer at the surface of the modified electrode [39]. Lower the ΔE_p, higher is the rate of electron transfer. The ΔE_p at HEA:G modified electrodes increases with HEA nanoparticle loading as mentioned in Table 2. However, for the 70:30 HEA:G composite there was a decrease in ΔE_p = 130 mV with maximum electroactive surface area [A_{eff}] as given in Table 2. The reduction in ΔE_p with increased surface area indicates the presence of heterogenous electro- catalytic active sites at a higher percentage leading to better electron transfer kinetics at the surface of the electrode. Further, this argument is supported by calculating the heterogeneous electron transfer (HET) rate (k^0) using ΔE_p and Nicolson analysis method [40]. The detailed calculation and the plot representing the HET (k^0) rate is provided in Fig S1 whereas the obtained k^0 values are mentioned in Table 2.

Fig. 6E represents the plot of anodic peak currents versus square root of the scan rate ($\upsilon^{1/2}$) for individual HEA:G composites. The linear increase in the anodic peak current corresponds to a diffusional controlled electrochemical process. The respective linear regression equations for the HEA:G composites - 20:80, 50:50, 70:30 and 90:10 are I_{pa}= 3.89x-0.45, I_{pa}= 3.85x – 0.56, I_{pa}= 4.60x – 1.49, I_{pa} = 2.85x – 0.03 respectively and derived slope values are tabulated (Table 2). The electroactive surface area of the modified electrodes with HEA:G composites was calculated using the Randles-Sevcik equation below [39].

$$I_p = \left(2.65 \times 10^5\right) n^{3/2} D^{1/2} \upsilon^{1/2} C A_{eff} \quad (3)$$

where n = number of electrons transferred during the electrochemical process, υ = scan rate, D = diffusion coefficient of the redox process, C is the concentration of the redox probe, A_{eff} is the electrochemically active surface area.

The calculated parameters ΔE_p at the scan rate of 10 mV/s, k^0(HET), A_{eff}, slope derived from forward peak currents are provided in Table 2. The 20:80 HEA:G composite exhibits better ΔE_p and HET (k^0). Further, with an increase in particle loading, there is an elevation in the ΔE_p (50:50) however, for the composite 70:30, there is a drop in ΔE_p with increased slope, A_{eff} and HET (k^0). Also, the nature of the cyclic voltammogram for the composite 90:10 is different compared to other composites indicating the prominence of composite ratios in the resulting electrochemical behavior. Hence, the HEA:G – 70:30 composite with 70 wt% HEA

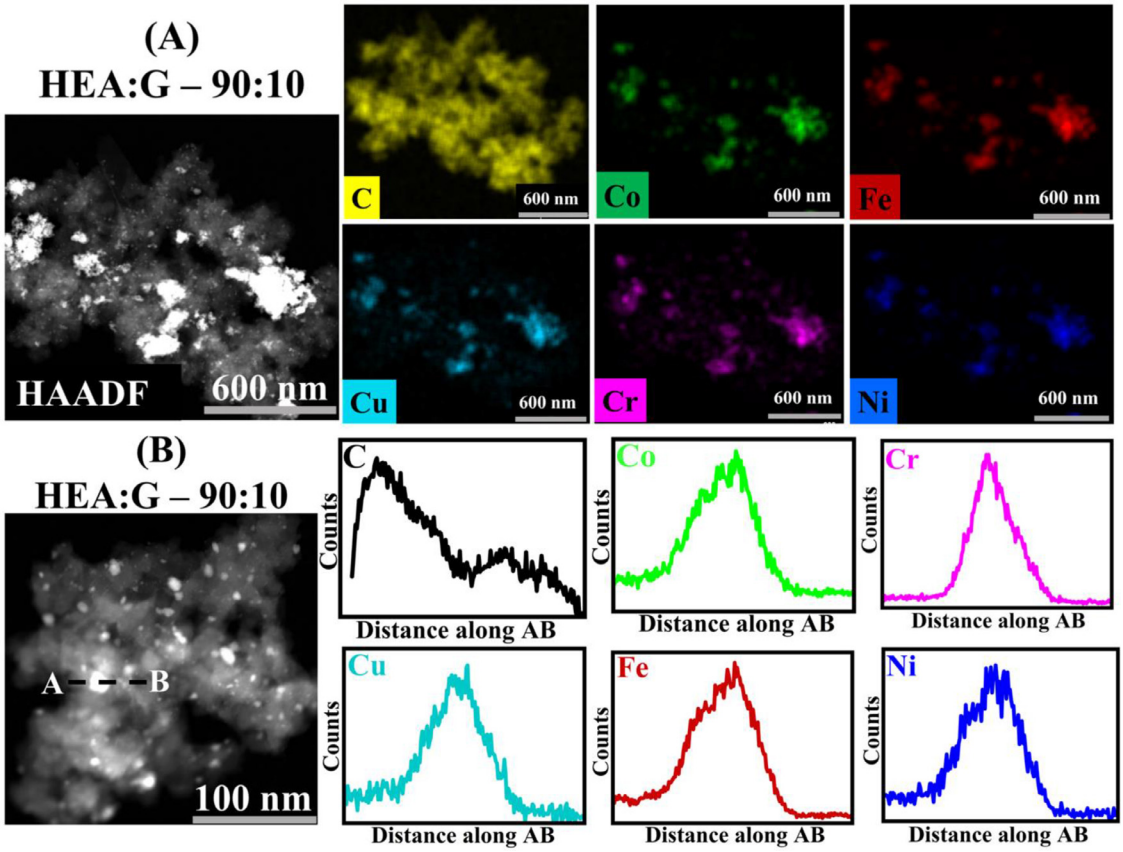

Fig. 5. Representative of HAADF – TEM (A) - compositional mapping and (B) - line profiles obtained for HEA-G composite – 90:10 confirming the presence of constituents (Co, Fe, Cr, Cu, Ni) of HEA nanoparticle on graphene (C).

Table 2
Representing the electrochemical behavior parameters against the redox probe $K_3Fe(CN)_6$.

HEA:G composites	ΔE_p(mV)	$A_{eff} \times 10^{-2}$ cm^2	I_p slope(μA)	$k^0 \times 10^{-2}$ cm s^{-1}
20:80	122.39	9.34	3.89	3.2
50:50	175.64	8.61	3.85	2
70:30	130	10.05	4.60	2.5
90:10	180.3	6.248	2.85	1.3

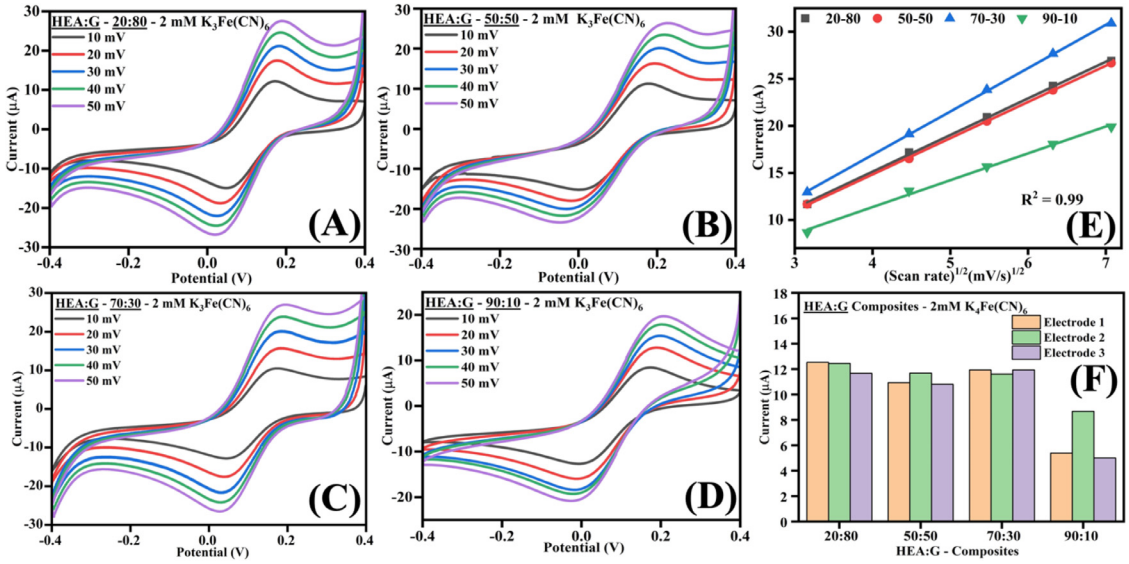

Fig. 6. (A – D) Cyclic voltammograms for the HEA:G composites against the redox probe $K_3Fe(CN)_6$. (E) Representing the linear plots of forward anodic current versus square root of the scan rate for the HEA:G composites. (F) Bar graphs indicating the forward peak currents obtained at the surface of the different electrodes prepared with HEA:G composites at same condition representing the reproducibility.

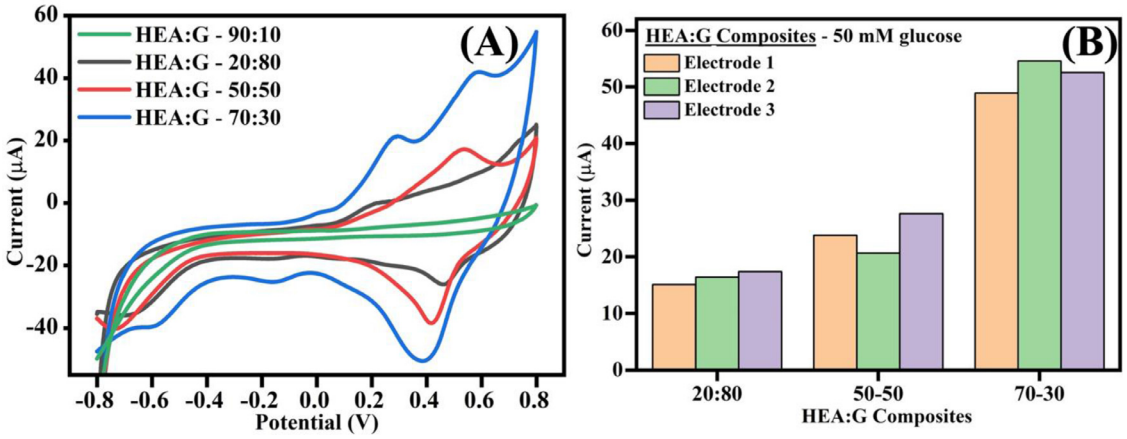

Fig. 7. (A) Cyclic voltammograms obtained for the HEA:G composites towards the oxidation of 50 mM glucose in 0.1 M PBS (B) Bar graphs indicating the oxidation currents against 50 mM glucose in 0.1 M PBS obtained at the surface of the different electrodes prepared with HEA:G composites at same condition representing the reproducibility.

nanoparticles and 30 wt% graphene can be considered as the optimum composition to achieve a better electrocatalytic activity.

3.2.1. Electro-oxidation of glucose on HEA:G composites

The catalytic ability of the HEA:G modified SPE electrodes has been further investigated towards the non-enzymatic detection of glucose. The cyclic voltammetry (CV) and differential pulse voltammetry (DPV) measurements were carried out to study electro-oxidation of glucose on HEA:G composite modified SPE electrodes in 0.1 M PBS as supporting electrolyte.

Cyclic voltammetry studies. Initially, CV was carried out between the potential range from −0.8 V to +0.8 V at the scan rate of 50 mV/s in the presence of 50 mM glucose in 0.1 M PBS. Fig. 7A shows cyclic voltammogram response of HEA:G composites 20:80, 50:50, 70:30 and 90:10. The 90:10 composite exhibits an insignificant response towards detection of glucose, whereas for 20:80, 50:50 and 70:30 composites, a significant peak representing the electro-oxidation of glucose can be observed. The rise in oxidation peak can be noticed beginning from 0.1 V. The oxidation current enhanced linearly with the composites 20:80, 50:50 and 70:30. The prominent oxidation peak for the HEA:G composites (Fig. 7A) were at 0.53 V for 20:80 and 50:50 whereas for 70:30 it was at 0.58 V. The corresponding oxidation currents for the composite 20:80, 50:50 and 70:30 was 18.15 μA, 27.95 μA, 52.46 μA respectively. In addition, two distinct oxidation peaks are observed, indicating two step oxidation process of glucose. The first peak between the range 0.3 V to 0.4 V corresponds to the oxidation of adsorbed glucose into intermediate product gluconolactone which is further oxidized to gluconic acid. Furthermore, the formation of hydroxyl layers (OHads) coincides with the electro-oxidation of glucose [41–43]. Therefore, the presence of a reduction peak ranging from 0.5 V to 0.4 V indicates hydroxyl layer reduction. However, there is no obvious metal oxidation or reduction due to the co-presence of metal components (Ni, Cu, Fe, Cr, Co) as a HEA alloy nanoparticle. Also, CV was carried out for the electrodes modified only with graphene (MG 100) and individual HEA nanoparticles. The plot representing the CV response is shown in the supplementary, Figs. S2 and S3 for MG 100 and HEA nanoparticles respectively. A similar significant redox response to glucose oxidation is not observed, indicating the importance of HEA:G composite catalytic behavior over their individual components. As a result, the HEA nanoparticle-graphene synergism plays a role in redox reactions.

The detection of glucose at HEA:G composites is in the order 90:10<20:80<50:50<70:30, hence for further experimental analysis only 20:80, 50:50 and 70:30 HEA:G composites were considered. Further, the measurements were carried out at three different trials for the composite 20:80, 50:50 and 70:30. Fig. 7B represents oxidation anodic currents obtained at 3 different electrodes in the detection of 50 mM glucose at 50 mV/s scan rate indicating a stable response. The CV measurements indicate the best catalytic behavior with HEA:G composite - 70:30 towards oxidation of glucose.

Scan rate and concentration dependency studies. To investigate the dynamic behavior of the modified electrodes with HEA:G composites, the CV measurements were carried out at different scan rates ranging from 10 mV/s to 50 mV/s in the presence of 50 mM glucose in 0.1 M PBS. Fig. 8A, 8B and 8C represent CV response for the composite 20:80, 50:50 and 70:30 respectively, at different scan rates. For all the three-composites, oxidation peak intensity and anodic current increases linearly with increasing scan rate. Fig. 8D represents linear anodic peak currents vs square root of the scan rates for all the three composites indicating that the electrochemical process on HEA:G composite modified electrodes is thermodynamically diffusional-controlled with the R^2 value between 0.98 to 0.99. The linear anodic current slope values derived from Fig.8D for HEA:G composites is in the order 20:80<50:50<70:30, with 70:30 exhibiting an enhanced performance compared to other composites with regards to the oxidation of glucose.

The sensing performance of the modified electrodes with HEA:G composites was investigated at varying concentrations of glucose (1 mM to 50 mM) in 0.1 M PBS at a fixed scan rate of 50 mV/s. Figs. 8E, 8F, 8 G represents the CV response obtained for the HEA:G composites 20:80, 50:50 and 70:30 respectively. The oxidation current linearly increased with an increase in the concentration of glucose correspondingly with all three composites. Fig. 8H represents a linear plot indicating the anodic current versus the concentration of the glucose for the composites 20:80, 50:50 and 70:30. The corresponding anodic slope values derived from Fig. 8H for the HEA:G composites is in the order 20:80<50:50<70:30. The anodic slopes corresponding to the sensitivity of the modified electrode with HEA:G composites was 0.117 μA mM^{-1} for 20:80, 0.2 μA mM^{-1} for 50:50 and 0.54 μA mM^{-1} for 70:30. Hence, 70:30 HEA:G exhibited the best sensing performance compared to 20:80 and 50:50.

3.2.2. Differential pulse voltammetry (DPV) analysis

The CV measurements indicate the onset of working potential which was due to the oxidation of glucose at around 0.1 V, however, 0.5 V was considered as the optimum potential because of the prominent rise in the anodic peak for the analysis. Hence,

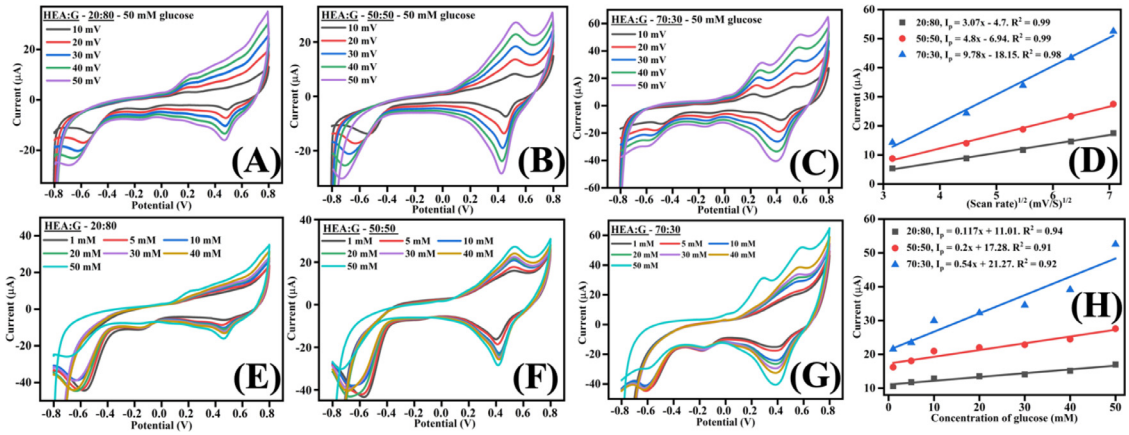

Fig. 8. (A - C) Cyclic voltammograms obtained for the HEA:G composites at different scan rates (10 mV/s to 50 mV/s) against 50 mM glucose in 0.1 M PBS. (D) Linear plot representing the oxidation current versus square root of the scan rate. (E-G) Cyclic voltammograms obtained for the HEA:G composites at different glucose concentrations (10 mM to 50 mM). (H) Representing the linear plot of oxidation current versus glucose concentration.

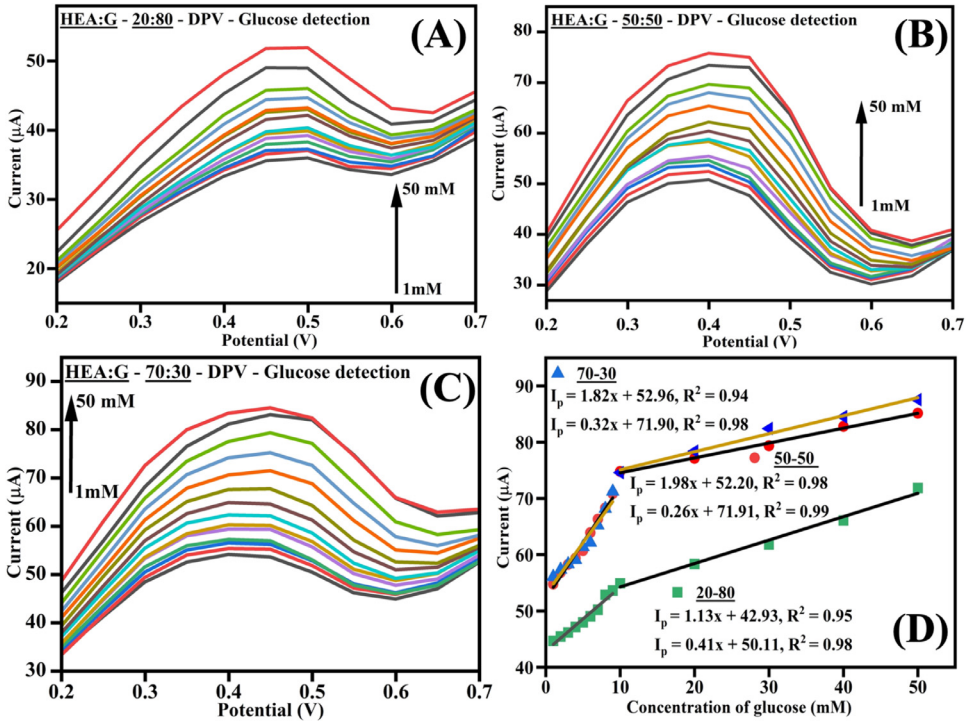

Fig. 9. (A – C) DPV response obtained for the HEA:G composites at different concentrations of glucose (1 mM to 50 mM). (D) Representing the linear plots of oxidation current versus concentration of glucose and corresponding linear regression equations for different HEA:G composites.

DPV being a quantitative measurement is performed to determine the working potential towards oxidation of glucose. The effect of capacitive current due to oxidation of glucose on the surface of the electrode is minimized in DPV and the resulting current is pure faradaic current corresponding to the concentration of glucose [44]. The DPV measurement was carried out at different concentrations of glucose (1 mM to 50 mM) in 0.1 M PBS at the scan rate of 100 mV/s. Fig. 9 (A, B and C) represents the DPV response obtained for the composites 20:80, 50:50 and 70:30 respectively. The intensity of the anodic oxidation peak indicates the working potential at 0.45 V for the composite 20:80 and at 0.4 V for the composite 50:50 and 70:30. The oxidation current increased as the concentration of the glucose increased for all three composites. Like the observation in CV measurements, the oxidation current from DPV response was in the order 20:80<50:50<70:30. The DPV measurements were carried out at three different trials for all the three HEA:G composites. Fig. 9D represents the average linear regression plots from three trials between the oxidation current and the concentration of glucose for the composites 20:80, 50:50 and 90:10. The derived slope values (Table 3) represents the sensitivity of the modified electrodes towards the oxidation of the glucose for the HEA:G composites. From Fig. 9D, the slopes representing the sensitivity of the electrodes indicates saturation between the composites 50:50 and 70:30. However, a significant sensitivity can be observed at the modified electrodes with HEA:G composites.

The addition of HEA nanoparticles on graphene substrates influences the enhancement of heterogenous electroactive sites

Table 3
Representing the sensitivity of the modified electrodes with HEA:G composites calculated from DPV measurements.

HEA:G composites	Operating potential (V)	Sensitivity ($\mu AmM^{-1}cm^{-2}$)
20:80	0.45	12.09 (10 – 50 mM)
	V	4.3897 (1 – 10 mM)
50:50	0.4	22.99 (10 – 50 mM)
	V	3.01 (1 – 10 mM)
70:30	0.4	18.2 (10 – 50 mM)
	V	3.2 (1 – 10 mM)

and accelerates the rate of electron transfer [19]. In general, electrochemically glucose oxidation is a two-step oxidation electron process that involves the oxidation of glucose to intermediate product gluconolactone and finally, to gluconic acid. This involves adsorption of glucose on the catalytic active sites which are oxidized to gluconolactone leading to electron transfer, followed by interfacial electron transfer from catalytic active material towards the substrate resulting in the final product [45,46]. Hence, HEA nanoparticles with a high surface to volume ratio act as an effective catalytic adsorption site contributing towards catalysis of glucose oxidation leading to electron transfer. The graphene substrates occupied with HEA nanoparticles and defects due to milling accelerate the rate of electron transfer, completing the process of glucose oxidation with increased sensitivity. The synergistic effect between the HEA nanoparticles and graphene as a composite is evident in glucose oxidation and the effectless of only the HEA nanoparticle and milled graphene (MG 100) indicates the importance of the composite. The unresponsive catalytic behavior of the HEA:G - 90:10 composite suggests the need for an optimum weight percentage of HEA nanoparticle and graphene content as a composite for exhibiting evident catalytic behavior.

4. Conclusion

The HEA-graphene composites at different weight percentage ratios were produced via a green approach i.e., Mechanical ball milling followed by sonication assisted exfoliation. The maintained weight ratios of metal powders were 20%, 50%, 70%, 90% and graphite was 80%, 50%, 30%, 10%. The produced HEA:G composites were 20:80, 50:50, 70:30 and 90:10. The structural characterization confirmed the formation of solid solution HEA nanoparticle on exfoliated few-layered graphene sheets. The variation in the HEA nanoparticle weight percent was evident with variation in the defect density and graphene crystalline size (Table 1). The electrochemical behavior of HEA:G composites for the redox probe $K_3Fe(CN)_6$ confirmed the improved electron transfer kinetics, enhanced redox currents followed by electrochemical active surface area with increase in the percentage of HEA nanoparticles. However, the HEA:G composite - 90:10 showed diminished performance indicating the importance of optimum weight percent of HEA:G composites. Further, 20:80, 50:50, 70:30 - HEA:G composites except 90:10 showed significant response towards electrochemical oxidation of glucose. The improved working potentials and linearly enhanced oxidation currents among HEA:G composites was found to be in the order 20:80>50:50>70:30. Also, for the comparison studies, individual HEA nanoparticle and milled graphene's electrochemical behaviors were studied which did not show any response, indicating the prominence of HEA:G composites with enhanced catalytic activity. Hence, only 20:80, 50:50 and 70:30 was considered to evaluate sensing ability towards non-enzymatic glucose detection. The composites exhibited good response with wide linearity and better sensitivity as reported. Hence, HEA:G composites can be a new class of material to explore in the area of non-enzymatic sensing applications.

Declaration of Competing Interest

The authors declare that they have no known competing financial interests or personal relationships that could have appeared to influence the work reported in this paper.

Acknowledgement

This work was supported by the KIRAN Division, Department of Science and Technology, Government of India under the Women Scientist Scheme-B (Project Grant No. DST/WOS-B/2018/2045/ETD/Ashwini). Funding from DST, the Government of India is also gratefully acknowledged.

Supplementary materials

Supplementary material associated with this article can be found, in the online version, at doi:10.1016/j.cartre.2022.100216.

References

[1] S. Hassasi, S.K. Hassaninejad-darzi, A. Vahid, Production of copper-graphene nanocomposite as a voltammetric sensor for determination of anti-diabetic metformin using response surface methodology, Microchem. J. 172 (2022) 106877, doi:10.1016/j.microc.2021.106877.
[2] Z. Wu, Y. Sun, Y. Tan, S. Yang, X. Feng, Three-Dimensional Graphene-Based Macro- and Mesoporous Frameworks for High-Performance Electrochemical Capacitive Energy Storage, J. Am. Chem. Soc. 134 (2012) 19532–19535, doi:10.1021/ja308676h.
[3] Z. Yan, W. Yao, L. Hu, D. Liu, Progress in the preparation and application of three-dimensional graphene-based porous nanocomposites, Nanoscale 7 (2015) 5563–5577, doi:10.1039/c5nr00030k.
[4] X. Zhang, D. Liu, L. Yang, L. Zhou, T. You, Self-assembled three-dimensional graphene-based materials for dye adsorption and catalysis, J. Mater. Chem. A. 3 (2015) 10031–10037, doi:10.1039/c5ta00355e.
[5] X. Fan, G. Jiao, W. Zhao, P. Jina, X. Li, Magnetic Fe3O4–graphene composites as targeted drug nanocarriers for pH-activated release, Nanoscale 5 (2013) 1143 –1142, doi:10.1039/c2nr33158f.
[6] H. Kim, D. Seo, S. Kim, J. Kim, K. Kang, Highly reversible Co_3O_4/graphene hybrid anode for lithium rechargeable batteries, Carbon N Y 49 (2010) 326–332, doi:10.1016/j.carbon.2010.09.033.
[7] S. Guo, S. Dong, E. Wang, Three-Dimensional Pt-on-Pd Bimetallic Nanodendrites Supported on Graphene Nanosheet : facile Synthesis and Used as an Advanced Nanoelectrocatalyst for Methanol Oxidation, 4 (2010) 547–555. https://doi.org/10.1021/nn9014483
[8] J. Zhang, X. Liu, L. Wang, T. Yang, X. Guo, S. Wu, S. Zhang, S. Wang, A simple one-pot strategy for the synthesis of ternary reduced graphite oxide /SnO 2 / Au hybrid nanomaterials, Carbon N. Y. 49 (2011) 3538–3543, doi:10.1016/j.carbon.2011.04.053.
[9] T. Baby, S. Ramaprabhu, Synthesis and nanofluid application of silver nanoparticles decorated, J.M. Chem 21 (2011) 9702–9709, doi:10.1039/c0jm04106h.
[10] H. Wu, J. Wang, X. Kang, C. Wang, D. Wang, J. Liu, I.A. Aksay, Y. Lin, Glucose biosensor based on immobilization of glucose oxidase in platinum nanoparticles /graphene / chitosan nanocomposite film, Talanta 80 (2009) 403–406, doi:10.1016/j.talanta.2009.06.054.
[11] W. Song, J. Xie, S. Liu, G. Cao, T. Zhu, Self-assembly of a $ZnFe_2O_4$/graphene hybrid and its application as a high-performance anode material for Li-ion batteries, New, J.Chem. 26 (2012) 2236–2241, doi:10.1039/C2NJ40534B.
[12] J. Liu, Q. Ma, Z. Huang, G. Liu, H. Zhang, Recent Progress in Graphene-Based Noble-Metal Nanocomposites for Electrocatalytic Applications, Adv. Mater. 1800696 (2019) 1–20, doi:10.1002/adma.201800696.
[13] C. Xu, A. Vasileff, B. Jin, D. Wang, .H. Xu, Y. Zheng, S. Qiao, Graphene-encapsulated nickel–copper bimetallic nanoparticle catalysts for electrochemical reduction of CO to CO_2. Chem, Commun. 56 (2020) 11275–11278, doi:10.1039/D0CC04779A.
[14] Y. Jin, X. Ding, L. Zhang, M. Cong, F. Xu, Y. Wei, S. Hao, Y. Gao, Boosting electrocatalytic reduction of nitrogen alloy engineering, 56 (2020) 11477–11480. https://doi.org/10.1039/d0cc02489a.
[15] H. Gao, F. Xiao, C.B. Ching, H. Duan, One-step electrochemical synthesis of PtNi nanoparticle-graphene nanocomposites for nonenzymatic amperometric glucose detection, ACS Appl. Mater. Interfaces. 3 (2011) 3049–3057, doi:10.1021/am200563f.
[16] Y. Xin, S. Li, Y. Qian, W. Zhu, H. Yuan, P. Jiang, R. Guo, L. Wang, High-Entropy Alloys as a Platform for Catalysis : progress, Challenges, and Opportunities, ACS Catal. 10 (2020) 11280–11306, doi:10.1021/acscatal.0c03617.
[17] W. Koo, J.E. Millstone, P.S. Weiss, I. Kim, The Design and Science of Polyelemental Nanoparticles, ACS Nano 14 (2020) 6407–6413, doi:10.1021/acsnano.0c03993.
[18] G.M. Tomboc, T. Kwon, J. Joo, K. Lee, High entropy alloy electrocatalysts: a critical assessment of fabrication and performance, J. Mater. Chem. A. 8 (2020) 14844–14862, doi:10.1039/D0TA05176D.

[19] H. Li, Y. Han, H. Zhao, W. Qi, D. Zhang, Y. Yu, W. Cai, S. Li, J. Lai, B. Huang, L. Wang, Fast site-to-site electron transfer of high-entropy alloy nanocatalyst driving redox electrocatalysis, Nat. Commun. 11 (2020) 5437, doi:10.1038/s41467-020-19277-9.
[20] Y. Chen, Y.Huang H.Fu, L. Huang, X. Zheng, Y. Dai, Y. Huang, W. Luo, Opportunities for High-Entropy Materials in Rechargeable Batteries, ACS Materials Lett. 3 (2021) 160–170, doi:10.1021/acsmaterialslett.0c00484.
[21] M.Y.Rekha R.Nandan, H.R. Devi, C. Srivastava, K.K. Nanda, High-entropy alloys for water oxidation: a new class of electrocatalysts to look out for, Chem. Commun. 57 (2021) 611, doi:10.1039/D0CC06485H.
[22] S. Singh, S.M. Shaikh, M.K.P. Kumar, B.S. Murty, C. Srivastava, Microstructural homogenization and substantial improvement in corrosion resistance of mechanically alloyed FeCoCrNiCu high entropy alloys by incorporation of carbon nanotubes, Materialia 14 (2020) 100917, doi:10.1016/j.mtla.2020.100917.
[23] A. Aliyu, C. Srivastava, Microstructure and corrosion properties of MnCrFeCoNi high entropy alloy-graphene oxide composite coatings, Materialia 5 (2019) 100249, doi:10.1016/j.mtla.2019.100249.
[24] D.G. Shin, H. Yeo, B.C. Ku, M. Goh, N.H. You, A facile synthesis method for highly water-dispersible reduced graphene oxide based on covalently linked pyridinium salt, Carbon N Y 121 (2017) 17–24, doi:10.1016/j.carbon.2017.05.064.
[25] W. Du, M. Wu, M. Zhang, G. Xu, T. Gao, L. Qian, X. Yu, F. Chi, C. Li, G. Shi, High-quality graphene films and nitrogen-doped organogels prepared from the organic dispersions of graphene oxide, Carbon N Y 129 (2018) 15–20, doi:10.1016/j.carbon.2017.11.077.
[26] X. Sun, L. Shi, H. Huang, X. Song, T. Ma, Surface engineered 2D materials for photocatalysis, Chem. Commun. 56 (2020) 11000–11013, doi:10.1039/D0CC04790B.
[27] P. Dash, T. Dash, T.K. Rout, A.K. Sahu, S.K. Biswal, B.K. Mishra, Preparation of graphene oxide by dry planetary ball milling process from natural graphite, RSC Adv 6 (2016) 12657–12668, doi:10.1039/C5RA26491J.
[28] L. Liu, A. Corma, Metal Catalysts for Heterogeneous Catalysis: from Single Atoms to Nanoclusters and Nanoparticles, Chem. Rev. 118 (2018) 4981–5079, doi:10.1021/acs.chemrev.7b00776.
[29] G.C. Ayala, M.C. Valadez, P.G.M. Gonzalez, R.B. Hurtado, J.I.C. Rascón, R.C.C. Torres, Ma.E. Zayas, S.J. Castillo, A.R.H. Martińez, M.F. Acosta, Green synthesis of reduced graphene oxide using ball milling, Carbon Lett 21 (2017) 93–97, doi:10.5714/CL.2017.21.093.
[30] B. Ye, C. An, Y. Zhang, C. Song, X. Geng, J. Wang, One-Step Ball Milling Preparation of Nanoscale CL-20/Graphene Oxide for Significantly Reduced Particle Size and Sensitivity, Nanoscale Res. Lett. (2018) 13–42, doi:10.1186/s11671-017-2416-y.
[31] D.W. Chang, H.J. Choi, I.Y. Jeon, J.M. Seo, L. Dai, Jong-Beom Baek, Solvent-free mechanochemical reduction of graphene oxide, Carbon. 77 (2014) 501–507. https://doi.org/10.1016/j.carbon.2014.05.055
[32] M.Y. Rekha, Nitin Mallik, Chandan Srivastava, First Report on High Entropy Alloy Nanoparticle Decorated Graphene, Sci. Rep. 8 (2018) 8737, doi:10.1038/s41598-018-27096-8.
[33] R. Ashwini, M.K. Punith Kumar, M.Y. Rekha, M.S. Santosh, Chandan Srivastava, Optimization of NiFeCrCoCu high entropy alloy nanoparticle – graphene (HEA-G) composite for the enhanced electrochemical sensitivity towards urea oxidation, J. Alloys Compd. 903 (2022) 163846, doi:10.1016/j.jallcom.2022.163846.
[34] A.L. Patterson, The Scherrer Formula for I-Ray Particle Size Determination, Physical Reviews 56 (1939) 978–982, doi:10.1103/PhysRev.56.978.
[35] Z. Ren, H. Mao, H. Luo, Y. Liu, Glucose sensor based on porous Ni by using a graphene bottom layer combined with a Ni middle layer, Carbon N Y 149 (2019) 609–617, doi:10.1016/j.carbon.2019.04.073.
[36] Y. Zhang, N. Li, Y. Xiang, D. Wang, P. Zhang, Y. Wang, S. Lu, R. Xu, J. Zhao, A flexible non-enzymatic glucose sensor based on copper nanoparticles anchored on laser-induced graphene, Carbon N Y 156 (2020) 506–513, doi:10.1016/j.carbon.2019.10.006.
[37] J. Hao, C. Li, C. Wu, K. Wu, In-situ synthesis of carbon-encapsulated Ni nanoparticles decorated graphene nanosheets with high reactivity toward glucose oxidation and sensing, Carbon N Y 148 (2019) 44–51, doi:10.1016/j.carbon.2019.03.048.
[38] M.M. Lucchese, F. Stavale, E.H.M. Ferreira, C. Vilani, M.V.O. Moutinho, R.B. Capaz, C.A. Achete, A. Jorio, Quantifying ion-induced defects and Raman relaxation length in graphene, Carbon N Y 48 (2010) 1592–1597, doi:10.1016/j.carbon.2009.12.057.
[39] A.J. Slate, D.A.C. Brownson, A.S. Abo Dena, G.C. Smith, K.A. Whitehead, C.E. Banks, Exploring the electrochemical performance of graphite and graphene paste electrodes composed of varying lateral flake sizes, Phys.Chem.Chem.Phys 20 (2018) 20010–20022, doi:10.1039/C8CP02196A.
[40] R.S. Nicholson, Theory and application of cyclic voltammetry for Measurement of Electrode Reaction Kinetics, Anal.Chem 37 (1965) 11, doi:10.1021/ac60230a016.
[41] H. Zhu, L. Li, W. Zhou, Z. Shao, X. Chen, Advances in non-enzymatic glucose sensors based on metal oxides, Mater. Chem. B. 4 (2016) 7333–7349, doi:10.1039/C6TB02037B.
[42] N. Schlegel, G.K.H. Wiberg, M. Arenz, On the electrooxidation of glucose on gold: towards an electrochemical glucaric acid production as value-added chemical, Electrochim. Acta 410 (2022) 14002, doi:10.1016/j.electacta.2022.140023.
[43] R. Reghunath, K. Devi, K.K. Singh, Recent advances in graphene based electrochemical glucose sensor, Nano-struct. & Nano-Objects 26 (2021) 1000750, doi:10.1016/j.nanoso.2021.100750.
[44] S.A. Abrori, N.L.W. Septiani, I.Anshori Nugraha, V.Suendo Suyatman, B. Yuliarto, Metal-Organic-Framework FeBDC-Derived Fe3O4 for Non-Enzymatic Electrochemical Detection of Glucose, Sensors 20 (2020) 4891, doi:10.3390/s20174891.
[45] S. Park, H. Boo, T.D. Chung, Electrochemical non-enzymatic glucose sensors, Anal.Chim. Acta. 556 (2006) 46–57, doi:10.1016/j.aca.2005.05.080.
[46] Lu Lu, Nanoporous noble metal-based alloys: a review on synthesis and applications to electrocatalysis and electrochemical sensing, Microchim. Acta. 186 (2019) 664, doi:10.1007/s00604-019-3772-3.